

# Discovery of Large-Scale Gravitational Infall in a Possible Massive Protostellar Cluster

Peter J. Barnes<sup>1,2</sup>, Yoshinori Yonekura<sup>3,4</sup>, Stuart D. Ryder<sup>5</sup>, Andrew M. Hopkins<sup>1,5</sup>,  
Yosuke Miyamoto<sup>6</sup>, Naoko Furukawa<sup>6</sup>, and Yasuo Fukui<sup>6</sup>

peterb@astro.ufl.edu

## ABSTRACT

We report Mopra (ATNF), Anglo-Australian Telescope, and Atacama Submillimeter Telescope Experiment observations of a molecular core in Carina, BY72 = G286.21+0.17, which give evidence of large-scale gravitational infall in the dense gas. From the millimetre and far-infrared data, the core has mass  $\sim 5,000 M_{\odot}$ , luminosity  $\sim 2\text{--}3 \times 10^4 L_{\odot}$ , diameter  $\sim 0.9$  pc, and mass infall rate  $\sim 2.4 \times 10^{-2} M_{\odot} \text{yr}^{-1}$ . If confirmed, this rate for gravitational infall in a molecular core may be the highest yet seen. The near-infrared  $K$ -band imaging shows an adjacent compact HII region and IR cluster surrounded by a shell-like photodissociation region showing  $\text{H}_2$  emission. At the molecular infall peak, the  $K$  imaging also reveals a deeply embedded group of stars with associated  $\text{H}_2$  emission. The combination of these features is very unusual and we suggest they indicate the ongoing formation of a massive star cluster. We discuss the implications of these data for competing theories of massive star formation.

*Subject headings:* astrochemistry — infrared: ISM — ISM: kinematics and dynamics — ISM: molecules — radio lines: ISM — stars:formation

---

<sup>1</sup>School of Physics A28, University of Sydney, NSW 2006, Australia

<sup>2</sup>Astronomy Department, University of Florida, Gainesville, FL 32611, USA

<sup>3</sup>Department of Physical Science, Osaka Prefecture University, 1-1 Gakuen-cho, Sakai, Osaka 599-8531, Japan

<sup>4</sup>Faculty of Science, Ibaraki University, 2-1-1 Bunkyo, Mito, Ibaraki 310-8512, Japan

<sup>5</sup>Anglo-Australian Observatory, PO Box 296, Epping, NSW 1710, Australia

<sup>6</sup>Department of Astrophysics, Nagoya University, Furo-cho, Chikusa-ku, Nagoya 464-8602, Japan

## 1. Introduction

Many details of massive star formation in dense molecular cores are still unclear (Churchwell 2002), despite much recent progress (e.g., Sridharan et al. 2002; Fuller et al. 2005; Longmore et al. 2007). For example, it is still being debated whether massive stars can form by a scaled-up version of the accretion thought to occur with low-mass protostars (e.g. McKee & Tan 2003), or rather form by collective processes in a clustered environment (e.g. Bonnell et al. 2003). Consequently, examples of massive star formation showing evidence of either behaviour can be informative to this debate, especially since there are still relatively few examples known of true massive protostars.

As part of the *Census of High- and Medium-mass Protostars* (CHaMP, see below), we identified the massive dense core G286.21+0.17 as showing striking evidence of large-scale gravitational infall, which we report here. This source (hereafter referred to as BY72, from the master CHaMP source list; Yonekura et al. 2008, in prep.) has been included in some previous surveys (Bronfman et al. 1996; Dutra et al. 2003; Faundez et al. 2004; Yonekura et al. 2005) and is an Infrared Astronomical Satellite (IRAS) point source, but has not previously been shown to be remarkable. The precise location is  $(l,b) = (286^\circ.208, +0^\circ.169)$  or  $(\alpha,\delta)_{J2000} = (10^h38^m32^s.2, -58^\circ19'12'')$ , about 1.5 northwest of  $\eta$  Carinae, at a kinematic distance of 2.2 kpc.

## 2. Observations

### 2.1. Survey Strategy

The motivation for CHaMP is to make a complete and unbiased census of higher-mass star formation at many different wavelengths over a large portion of the Milky Way (Barnes et al. 2006), in order to systematically characterise the processes in massive star formation in a uniform way. The first step was to identify 171 dense clumps from  $C^{18}O$  and  $HCO^+$  maps made with the 4m Nanten telescope (Yonekura et al. 2005, 2008) of a  $20^\circ \times 6^\circ$  region of the Galactic Plane in Vela, Carina, and Centaurus (specifically  $300^\circ > l > 280^\circ$  and  $-4^\circ < b < +2^\circ$ ). A higher-resolution follow-up campaign was then begun to map these cores in a number of 3-millimetre wavelength (3mm) molecular transitions with the 22m-diameter Mopra dish of the Australia Telescope National Facility<sup>1</sup> (Barnes et al. 2008). The

---

<sup>1</sup>The Mopra telescope is part of the Australia Telescope which is funded by the Commonwealth of Australia for operation as a National Facility managed by CSIRO. The University of New South Wales Digital Filter Bank used for the observations with the Mopra telescope was provided with support from the Aus-

Mopra antenna’s performance has been described by Ladd et al. (2005). Since that study, an on-the-fly (OTF) mapping capability has been implemented in the control software (in 2004), new 3mm MMIC receivers were installed (in 2005) which were at least as sensitive as the previous SIS mixers and much more efficient to operate, and the MOPS wideband digital filterbank was commissioned (in 2006; Wilson et al. 2006). This latter innovation especially, when combined with the Nanten maps as finder charts, makes an ambitious survey like CHaMP possible.

The MOPS backend allows up to sixteen independently selectable 137-MHz-wide “zoom modes,” from within the filterbank’s 8 GHz total instantaneous bandwidth, to be observed simultaneously. Each zoom mode is correlated with 4096 channels in each of two orthogonal polarisations, resulting in a spectral resolution of 33 kHz, or  $0.11 \text{ km s}^{-1}$  at 90 GHz. In the 2006 and 2007 austral winter seasons we mapped the brightest  $\sim 120$  Nanten clumps, simultaneously covering many spectral lines in the 85–93 GHz range, among them the  $J=1\rightarrow 0$  transitions of  $\text{HCO}^+$ ,  $\text{HCN}$ ,  $\text{N}_2\text{H}^+$ ,  $\text{H}^{13}\text{CO}^+$ , and  $\text{H}^{13}\text{CN}$ . At these frequencies, Mopra has a half-power beamwidth of  $36''$  and aperture and beam efficiencies of 0.5 and 0.7, respectively (Ladd et al. 2005).

While CHaMP’s 3mm molecular maps reveal ongoing star formation activity, complementary near-IR imaging of the same cores can show where star formation has progressed to a more evolved state. By compiling these statistics uniformly we will be in an excellent position to identify demographic trends in the massive star formation process. Thus, an equally important part of CHaMP is a near-IR survey of the Nanten clumps using the IRIS2 imager (Tinney et al. 2004) on the Anglo-Australian Telescope (AAT). With this instrument we have begun acquiring images of each core in  $K$ -continuum, Brackett- $\gamma$  (a recombination line tracing HII regions), and  $\text{H}_2 v=1\rightarrow 0 S(1)$  &  $v=2\rightarrow 1 S(1)$  (vibrational quadrupole lines tracing molecular gas heated to a few 1000 K) to delineate the relationship between formed and forming massive stars, and report here the results of this imaging.

A third major component of CHaMP will be a deep imaging survey of 1.2mm continuum and spectral-line emission with Atacama Submillimeter Telescope Experiment (ASTE), the 10m submillimeter telescope of the Nobeyama Radio Observatory<sup>2</sup> at Pampa la Bola in Chile (Kohno et al. 2004; Ezawa et al. 2004). The half-power beamwidth of the telescope is

---

tralian Research Council.

<sup>2</sup>The ASTE project is led by Nobeyama Radio Observatory (NRO), a branch of National Astronomical Observatory of Japan (NAOJ), in collaboration with the University of Chile and Japanese institutes including the University of Tokyo, Nagoya University, Osaka Prefecture University, Ibaraki University, Kobe University, and Hokkaido University.

22'' at 345 GHz and the front end is a 4 K cooled SIS mixer receiver (Kohno 2005). The 1mm continuum is important in characterising the spectral energy distributions (SEDs) of embedded protostars as well as starless cores, and in correlating this with the phenomenology seen in spectral lines and at other wavelengths. We report here as well some of the first data from this facility, namely HCO<sup>+</sup> and H<sup>13</sup>CO<sup>+</sup>  $J=4\rightarrow3$  spectra, confirming the evidence of infall from our Mopra data.

## 2.2. Observational Details and Data Reduction

The evidence for infall in BY72 was first seen in the Mopra HCO<sup>+</sup> and H<sup>13</sup>CO<sup>+</sup>  $J=1\rightarrow0$  data, presented in Figures 1–4. These were obtained on 2006 Oct 27–29 and 2007 Sep 5–9, when observing conditions were good ( $T_{sys} \sim 300$  K or better). The images were formed by coadding 5'  $\times$  5' OTF maps which abut each other to cover larger areas. Each 5'  $\times$  5' area was scanned at least once each in  $l$  and  $b$  in order to minimise rastering artefacts. The raw OTF data were processed with the Livedata-Gridzilla package (Barnes et al. 2001) by bandpass division and baseline subtraction. The 2s-long OTF samples were then regridded onto a regular grid of 12'' pixels, where the samples were weighted by  $T_{sys}^{-2}$ , before averaging them into each gridded pixel. For all Mopra maps in Figures 1–5, the effective telescope HPBW has been smoothed at the gridding stage to 40'' from the intrinsic 36'', in order to reduce noise artefacts. The resulting spectral line data cubes have rms noise levels  $\sim 0.2$  K per 0.11 km s<sup>-1</sup> channel. Although the pointing (checked on the SiO maser source R Carinae every hour or two) was typically good to 10'' or better ( $< 1$  pixel on the scale of our maps), because of the simultaneity of the spectral line mapping afforded by MOPS, the relative registration of features between these lines is perfect.

Observations of HCO<sup>+</sup> and H<sup>13</sup>CO<sup>+</sup>  $J=4\rightarrow3$  were made using ASTE on 2006 Dec 1–2, when the typical system temperature (double-sideband) ranged from 220 K to 580 K at 345 GHz, including the atmosphere. We used a digital correlator with a bandwidth of 128 MHz and 1024 channels (Sorai et al. 2000). The effective spectral resolution was 151.25 kHz, corresponding to a velocity resolution of 0.13 km/s at 345 GHz. The data were obtained in position switching mode. Observations were made remotely from an ASTE operation room in San Pedro de Atacama, Chile, using a network observation system, N-COSMOS3, developed by NAOJ (Kamazaki et al. 2005). For HCO<sup>+</sup> and H<sup>13</sup>CO<sup>+</sup>, the total integration times of the spectra were 180s and 620s, and the rms noise levels 0.57 and 0.21 K per channel, respectively. The intensity was calibrated by using a room-temperature chopper wheel. The absolute intensity was calibrated by observing Orion-KL and assuming  $T_R^*(\text{HCO}^+) = 47$  K and  $T_R^*(\text{H}^{13}\text{CO}^+) = 2$  K (Schilke et al. 1997). The pointing accuracy was measured to be

reliable within  $5''$  as checked by optical observations of a star with a CCD camera attached to the telescope, as well as by CO  $J=3\rightarrow 2$  observations of IRC+10216.

IRIS2 observations were made at the AAT in service mode on 2006 May 13 in the  $K$ -band continuum ( $2.25\text{--}2.29\ \mu\text{m}$ ) and 3 spectral line filters as described above, Br- $\gamma$  and H<sub>2</sub>  $S(1)\ v=1\rightarrow 0$  &  $v=2\rightarrow 1$ . For each filter, nine 60s images (dithered by  $1'$ ) were obtained of the instrument’s  $7'.7\times 7'.7$  field under  $0''.9$  seeing, and reduced using the ORAC-DR data reduction pipeline (Cavanagh et al. 2003). However the conditions during the observations were non-photometric, there being a fair amount of bushfire haze present. Subsequent image processing was performed with the IRAF<sup>3</sup> package. The images for each field were registered using astrometry derived from SuperCOSMOS<sup>4</sup> I-band images; we estimate the resulting rms positional accuracy in the IRIS2 images to be  $< 0''.3$ . Next, we linearly scaled the spectral-line images to the same relative brightness scale as the  $K$ -band continuum by matching the integrated fluxes of several stars in each filter, assuming they were of similar colour. We then subtracted the continuum from the spectral-line images before transforming each image to Galactic coordinates. Finally, a three-colour image (shown in Fig. 5) was formed from the continuum-subtracted Br- $\gamma$  and H<sub>2</sub> images: Br- $\gamma$  is shown as red, and H<sub>2</sub>  $S(1)\ v=1\rightarrow 0$  &  $v=2\rightarrow 1$  are shown as green & blue, respectively.

Long-slit spectroscopy with IRIS2 was obtained on 2007 Oct 18. The  $7'.7$  long slit was set to a position angle of  $131^\circ.2$ , with the stellar cluster and nebulosity of BY72 spanning most of one half of the slit. Four exposures of 300s were obtained in the  $K$ -band, with BY72 nodded by  $3'.8$  along the slit between each exposure. Similar nodded exposures of the nearby A0V star HD 95534 were obtained to assist with telluric correction. All frames were flatfielded using quartz lamp exposures, then nodded pairs were subtracted to remove sky emission. After two-dimensional wavelength calibration and straightening with Xe lamp exposures, the “off” beam data were inverted, aligned, and co-added to the “on” beam data. Each spectral row of the BY 72 data was divided by an extracted spectrum of HD 95534 (from which intrinsic Br- $\gamma$  absorption had been removed), then multiplied by a blackbody spectrum of  $T_{eff} = 9520\ \text{K}$ .

---

<sup>3</sup>IRAF is distributed by the National Optical Astronomy Observatories, which are operated by the Association of Universities for Research in Astronomy, Inc., under cooperative agreement with the U.S. National Science Foundation.

<sup>4</sup>This research has made use of data obtained from the SuperCOSMOS Science Archive, prepared and hosted by the Wide Field Astronomy Unit, Institute for Astronomy, University of Edinburgh, which is funded by the UK Science and Technology Facilities Council.

### 3. Analysis and Discussion

#### 3.1. Evidence for Gravitational Infall

We assign a distance to BY72 of 2.2 kpc, based on the rotation curve of Clemens (1985) rescaled to  $R_0 = 8$  kpc and  $\Theta_0 = 200$  km s<sup>-1</sup> (Merrifield 1992) and noting that the molecular lines’ central  $V_{LSR} = -19.7$  km s<sup>-1</sup> is forbidden at this longitude, but only by a small amount ( $\sim 2$  km s<sup>-1</sup>, less than half the molecular cloud velocity dispersion around the mean Galactic rotation). This makes a location at the tangent distance likely.

The dense molecular core, centred at  $(l, b) = (286.208, +0.169)$  and easily visible in the Mopra maps, has HCO<sup>+</sup> spectral line profiles that fit the canonical pattern of Zhou et al. (1993) indicating gravitational infall onto a protostar (see Fig. 4). For the optically thick HCO<sup>+</sup> emission, this includes a self-absorbed profile with predominantly stronger blue wings at most positions (the “blue asymmetry” or inverse P-Cygni profile, seen in panels *a* and *c-g* of Fig. 4), together with more gaussian line profiles for the optically thin transitions of H<sup>13</sup>CO<sup>+</sup>, which are centred in velocity on the HCO<sup>+</sup> self-absorption (panels *b* and *h*). Further, the  $J=4\rightarrow 3$  lines (panels *g* and *h*) are brighter than the corresponding  $J=1\rightarrow 0$  lines (panels *a* and *b*), the self-absorption in the HCO<sup>+</sup> is deeper in the  $J=1\rightarrow 0$  than the  $J=4\rightarrow 3$ , the velocity difference  $V_{blue} - V_{red}$  (see below) between the blue and red peaks of the HCO<sup>+</sup> lines is slightly greater in the  $J=1\rightarrow 0$  than the  $J=4\rightarrow 3$ , and the blue and red peaks in the  $J=4\rightarrow 3$  line are both slightly blueward of the respective peaks in the  $J=1\rightarrow 0$  line. All of these details are completely consistent with the Zhou et al. (1993) and Myers et al. (1996) picture of a dense core undergoing gravitational infall, where the velocity of the infall and the temperature both increase towards the centre, producing the respective line profiles and ratios. The line profiles of the other bright species mapped at Mopra, such as HCN and N<sub>2</sub>H<sup>+</sup> (not shown here), are also consistent with this picture, after allowance is made for their hyperfine structure and different optical depths.

However, the mass scale of the infall appears to be unusual. Myers et al. (1996) developed a simple but useful model to evaluate basic parameters for molecular cores which are undergoing gravitational infall. Although their model was developed in the context of low-mass protostars, the results we derive here satisfy the assumptions made in their treatment of the radiative transfer. Using their formalism, we can use the HCO<sup>+</sup> line profiles to make estimates of the characteristic gas infall speed. From their eqn. (9) and using the parameters  $V_{blue} = -21.0 \pm 0.1$  km s<sup>-1</sup>,  $V_{red} = -18.0 \pm 0.1$  km s<sup>-1</sup>,  $T_D = 0.44 \pm 0.02$  K,  $T_{BD} = 1.10 \pm 0.04$  K,  $T_{RD} = 0.24 \pm 0.04$  K (all from Fig. 4a), and  $\sigma = 1.15 \pm 0.05$  km s<sup>-1</sup> from Figure 4b, we obtain  $V_{in} = 0.50 \pm 0.08$  km s<sup>-1</sup> using the  $J=1\rightarrow 0$  lines. Similarly for the  $J=4\rightarrow 3$  lines in Figures 4g and h,  $V_{blue} = -19.7 \pm 0.1$  km s<sup>-1</sup>,  $V_{red} = -17.8 \pm 0.1$  km s<sup>-1</sup>,

$T_D = 3.6 \pm 0.1$  K,  $T_{BD} = 2.6 \pm 0.2$  K,  $T_{RD} = 0.9 \pm 0.2$  K, and  $\sigma = 1.02 \pm 0.06$  km s<sup>-1</sup>, yielding  $V_{in} = 0.31 \pm 0.06$  km s<sup>-1</sup>.

Continuing to follow Myers et al., we need an estimate for the radius over which the infall profile is seen, in order to allow calculation of a kinematic mass infall rate. This profile is widespread in the HCO<sup>+</sup> data, but its intensity drops only slowly into the background, showing no hard edge. Therefore in what follows we use the emission FWHMs to give a radius. In the HCO<sup>+</sup> and H<sup>13</sup>CO<sup>+</sup>  $J=1 \rightarrow 0$  data,  $D_{FWHM} = 97'' \pm 12''$  and  $77'' \pm 12''$  respectively, taking a geometric mean of the major and minor axes in each case. Since these are so close, we take a simple mean between the two species to give  $R = 0.46 \pm 0.06$  pc for the core radius. This finally gives

$$\begin{aligned} \frac{dM_k}{dt} &= 4\pi R^2 \mu n_{cr} V_{in} \\ &\sim (2.4 \pm 0.7) \times 10^{-2} M_{\odot} \text{yr}^{-1} \end{aligned} \quad (1)$$

for BY72's mass infall rate, where  $\mu = 2.30$  is the mean molecular mass in the gas and  $n_{cr}$  is the critical density for the  $J=1 \rightarrow 0$  transition (see §3.2). This should be compared to the gravitational mass infall rate for the self-similar singular isothermal sphere (SIS) solution (Shu 1977)

$$\frac{dM_g}{dt} = \frac{\sigma^3}{G} \sim 0.04 \times 10^{-2} M_{\odot} \text{yr}^{-1}, \quad (2)$$

where instead of the sound speed  $c$  of Shu, we have substituted the turbulent velocity indicated by the linewidth  $\sigma$ , as suggested by Banerjee & Pudritz (2007). Even so, we see that for BY72, Shu's solution cannot give us the observed infall rate. Instead, Banerjee & Pudritz show that a magnetised core can collapse supersonically with an effective speed  $Mc$ , where  $M$  is the Mach number in the flow. For BY72, then, the observed infall only requires collapse with  $M \sim 4$ . The observed kinematic rate would in that case be consistent with the MHD simulations of Banerjee & Pudritz (2007); it is also consistent with the infall rates predicted by the McKee & Tan (2003) massive turbulent core model.

Myers et al. (1996) also suggested that, for their low-mass protostars, the agreement of the inferred and theoretical rates indicates the derived inward motions are consistent with gravitational infall. Under this interpretation BY72 gives a much larger infall rate than is typical of low-mass protostars ( $\sim 10^{-6} M_{\odot} \text{yr}^{-1}$ , increasing to  $10^{-4}$  to  $10^{-5} M_{\odot} \text{yr}^{-1}$  during FU Orionis-type outbursts; Lada 1999), and stems mainly from the large linear extent of the asymmetric HCO<sup>+</sup> profile ( $D \sim 1$  pc), and also from the unusually large value for

$V_{in}$ . This mass infall rate is also larger than any seen so far in any similar massive star-forming region (e.g. Fuller et al. 2005; Beltrán et al. 2006). Given the linear size of this region and the near-IR appearance of embedded cluster(s) within the cloud, we suspect that the entire BY72 cloud is undergoing a global gravitational collapse. Verification of this suggestion awaits additional supporting evidence including interferometric observations and more detailed modelling. It is worth noting that all of the Mopra spectral line maps of BY72 (e.g. HCN,  $N_2H^+$ , etc.), as well as the CS  $J=2\rightarrow 1$  data reported by Bronfman et al. (1996), show similar emission distributions and/or line profiles, with differences as expected from the species’ different relative abundance. This is not surprising considering that they all require high densities ( $n_{cr} \sim 10^{5-6} \text{ cm}^{-3}$ ; Spitzer 1978) to be collisionally excited and thermalised to the gas kinetic temperature, and so should reflect the same dynamical state as seen in the  $HCO^+$ .

### 3.2. Core Mass

In order to make a strong case for the formation of a massive cluster, we also need to establish that the molecular cloud and core have sufficient mass to qualify for this status. Since the gas density will probably be at least the critical value where the bright molecular emission is seen, a lower limit to the cloud mass is given approximately by

$$\begin{aligned}
 M &> \mu m_H n_{cr} (4\pi/3) R^3 \\
 &\sim 47,000 M_\odot \left( \frac{n_{H_2}}{3 \times 10^5 \text{ cm}^{-3}} \right) \left( \frac{R}{0.46 \text{ pc}} \right)^3
 \end{aligned}
 \tag{3}$$

using the  $HCO^+$   $J=1\rightarrow 0$  transition’s critical density (Haese & Woods 1979; Barnes & Crutcher 1990). Indeed, with ASTE’s detection of the  $J=4\rightarrow 3$  line, even higher-density gas ( $\sim 10^7 \text{ cm}^{-3}$ ) must exist in the core, and if widespread would give a much higher mass estimate. However eq. (3) assumes that the dense gas giving rise to the emission fills our beam, whereas the filling factor  $f$  is unknown and possibly  $\ll 1$ .

A formally more rigorous, but not necessarily more precise, mass estimate is made (and we obtain an estimate for  $f$  as well) if we use the  $HCO^+/H^{13}CO^+$  line ratio to estimate the optical depth  $\tau$  in the  $J=1\rightarrow 0$  line, and the  $HCO^+$   $J=4\rightarrow 3/1\rightarrow 0$  brightness ratio to estimate the excitation temperature in the dense gas. Assuming an excitation temperature



$T_{ex}$  under LTE, we obtain a column density for *each line of sight* from

$$N(\text{HCO}^+) = \frac{3k}{8\pi^3\nu\mu^2} \frac{T_r Q(T_{ex}) e^{E_u/kT_{ex}}}{1 - e^{-h\nu/kT_{ex}}} \int \tau dV \text{cm}^{-2}, \quad (4a)$$

(Townes & Schawlow 1975) where  $T_r = T_A^*/\eta$  is the peak brightness temperature in the line,  $Q$  is the partition function for  $\text{HCO}^+$  at the excitation temperature  $T_{ex}$ , and the line optical depth  $\tau$  (peak value  $\sim 6$  from the previous section) is integrated over the velocity (measured in  $\text{km s}^{-1}$ ), here taken over the range  $-23.2$  to  $-16.6 \text{ km s}^{-1}$  (as in Fig. 2).

Determining the excitation temperature is a little more complicated, however. Faundez et al (2004) derive  $T_d = 30 \text{ K}$  for the continuum dust emission from BY72, but found it necessary to fit two temperature components to the spectral energy distributions (SEDs) of most of their sources. They do not give an explicit value for the warm component in BY72, but their average warm component has  $T_d \sim 140 \text{ K}$ . From the  $\text{HCO}^+$   $J=4 \rightarrow 3/1 \rightarrow 0$  brightness ratio ( $\sim 2.6$ ) at the peak of BY72, we fit a  $T_{ex}$  closer to  $210 \text{ K}$  for the dense gas. Without a spatially-resolved  $\text{HCO}^+$   $J=4 \rightarrow 3$  map, we are limited to saying that the gas  $T_{ex}$  probably has a range of values from  $30\text{--}200 \text{ K}$ . At these  $T_{ex}$ ,  $Q \sim 14 - 98$ , giving

$$\begin{aligned} N(\text{HCO}^+) &= 1.13 \times 10^{11} \frac{T_r Q(T_{ex}) e^{E_u/kT_{ex}}}{1 - e^{-h\nu/kT_{ex}}} \int \tau dV \text{cm}^{-2} \\ &\sim 4 - 30 \times 10^{13} \text{cm}^{-2}, \end{aligned} \quad (4b)$$

Now, integrating this over the emission region yields a total cloud mass

$$\begin{aligned} M_{LTE} &= \frac{N}{X} (\mu m_H) \pi R^2 \\ &\sim 1500 - 12,000 M_\odot \frac{(R/0.46 \text{ pc})^2}{(X/3 \times 10^{-10})} \end{aligned} \quad (5)$$

The lower limit is certainly too low, since it doesn't include the contribution to the mass from the warmer (and presumably denser) component. However the upper limit is probably too high, since it is likely that such a warm temperature would not be typical of the whole parsec-wide dense clump. We estimate that an intermediate value,  $M \sim 5000 M_\odot$ , is probably reasonable.

In eq. (5) we have used an abundance  $X = 3 \times 10^{-10}$  for  $\text{HCO}^+$  relative to  $\text{H}_2$ , from recent models of massive core chemistry (e.g., Garrod et al. 2008). The models show  $X_{\text{HCO}^+}$  is a strong function of time, and is not necessarily the main charge carrier in such regions. Thus  $X_{\text{HCO}^+}$  in massive cores may be lower than a more typical value  $\sim 10^{-9}$  in low-mass cores (e.g., Loren et al. 1990; Caselli et al. 2002; Lee et al. 2003). Despite this uncertainty, eqs. (3) and (5) suggest that  $f$  may be small ( $\sim 0.1$ ), but that  $M$  is large.

Are there alternatives for the dynamical state of this core besides gravitational infall? To answer this, we evaluate a number of terms from the Virial Theorem. If the linewidths seen in the  $\text{HCO}^+$  ( $\sim 2 \text{ km s}^{-1}$  relative to the line centre, counting emission out to the half-power level) were due to rotational support against self-gravity (an interpretation we do not favour due to the self-absorbed line profiles fitting the expected infall shapes), then

$$\begin{aligned} M_{rot} &= v^2 R / G \\ &\sim 430 M_{\odot} \left( \frac{v}{2 \text{ km s}^{-1}} \right)^2 \left( \frac{R}{0.46 \text{ pc}} \right). \end{aligned} \tag{6a}$$

However thermal and magnetic pressure must also contribute to the support of the cloud; the corresponding virial relations give

$$\begin{aligned} M_{th} &= 5kT_{ex}R/m_{\text{H}_2}G \\ &\sim 70 M_{\odot} \left( \frac{T_{ex}}{30 \text{ K}} \right) \left( \frac{R}{0.46 \text{ pc}} \right) \end{aligned} \tag{6b}$$

and

$$\begin{aligned} M_{mag} &= (5B^2R^4/18G)^{1/2} \\ &\sim 300 M_{\odot} \left( \frac{B}{50 \mu\text{G}} \right) \left( \frac{R}{0.46 \text{ pc}} \right)^2, \end{aligned} \tag{6c}$$

where we have taken a typical value for the magnetic field in the molecular gas from studies in other similar regions (Crutcher 1999). These terms, even in combination ( $\sim 800 M_{\odot}$ ), are much too small to provide the necessary support against gravity, unless (for example) the magnetic field strength were at least ten times the value assumed here, and/or we take linewidths out to the zero-power level ( $\pm 4 \text{ km s}^{-1}$ ). While such values for rotation and the magnetic field are not entirely ruled out as a means of supporting BY72 against collapse,

they would be quite extreme. We infer that virial equilibrium does not apply in this case (HCO<sup>+</sup> abundance and  $T_{ex}$  uncertainties aside).

There is also the possibility that the velocity pattern in BY72 represents a massive outflow rather than infall. Besides the detailed spectroscopic arguments for infall, we discount the outflow interpretation since maps of the HCO<sup>+</sup> line wings (not shown here) do not reveal any particular geometric pattern, such as a strongly bipolar separation of the line wings. Nevertheless, sensitive <sup>12</sup>CO observations should be made of BY72, since they would be better able to find any outflow, if present.

The conclusion that BY72 is indeed a massive dense core undergoing contraction at least (if not collapse) seems fairly reliable, the strongest evidence being the line profiles and the IR appearance (see §3.3). Our mass estimate for BY72 compares well with others in the literature. For example, from Nanten CO mapping and IRAS fluxes, Yonekura et al. (2005) obtained LTE and virial cloud masses of 1900 and 3600 M<sub>⊙</sub> (resp.) and a luminosity  $3.0 \times 10^4 L_{\odot}$ . Our LTE mass estimate is larger than theirs, due to our use of a tracer of denser gas, but our virial mass is smaller than theirs, as expected with a smaller observed linear size and linewidth. From 1.2mm mapping and SED fitting Faundez et al. (2004) obtained a core mass of 470 M<sub>⊙</sub>, density  $n_{H_2} = 1.4 \times 10^5 \text{cm}^{-3}$ , dust temperature 30 K, and luminosity  $1.9 \times 10^4 L_{\odot}$ . Their mass value seems somewhat low, but could be as much as five times higher with a lower assumed dust opacity, as they point out. This would bring it into closer agreement with our LTE mass estimate, and suggests that such lower dust opacities may be required to explain the higher molecular masses.

### 3.3. Infrared Features

Our  $K$ -band imaging has much higher angular resolution than our mm data, or archival centimeter-wave (cm) and far-infrared (FIR) data, and shows some striking structures and correlations. Near the molecular core, there is a compact HII region (visible as a Br- $\gamma$  emission nebula) and IR cluster (visible also in the  $K$ -continuum image). The Br- $\gamma$  is exactly coincident with a 61 mJy  $\text{bm}^{-1}$  point source in the 843 MHz continuum from the Molonglo Galactic Plane Survey-2 (the MGPS-2 has a similar beamsize,  $45'' \times 53''$ , to our Mopra data; Murphy et al. 2007). Both such features have been seen before around similar massive star-forming dense cores, e.g. NGC 2024 (Barnes et al. 1989) or AFGL 5179 (Tej et al. 2006), but the example of BY72 is interesting in the rather clean separation of the ionised and molecular components, and the distinct “cocooning” of the excited H<sub>2</sub> emission around the very symmetric Br- $\gamma$  and cm-continuum. Indeed, this is actually reminiscent of planetary nebulae (e.g., Fig. 9 of Ryder et al. 1998) or the classic picture of a Strömgren sphere. From

the pseudocolour composite image in Fig. 5a, we see that the shell of excited  $\text{H}_2$  appears to be traced much better by the  $v=2\rightarrow 1$  than the  $v=1\rightarrow 0$  emission. This is surprising since a  $[1-0]/[2-1]$  ratio less than unity would be at odds with our understanding of  $\text{H}_2$  excitation. Instead, this ratio is likely either an artefact of differential reddening between the various filters used, or due to non-photometric imaging conditions, or both.

To confirm this we obtained a  $K$ -band long-slit spectrum aligned between the mm and Br- $\gamma$  peaks (Fig. 6), which shows that the  $[1-0]/[2-1]$  ratio is actually  $>1$  at the molecular-ionised interface, typical of photodissociation regions (PDRs) or shock-excited jets (e.g., Allers et al. 2005; Caratti o Garatti et al. 2006). From the measured  $S(1)$   $[1-0]/[2-1]$  ratio and the tabulation of Burton (1987), the gas temperature at the PDR interface is constrained to be  $>4000$  K; including the  $S(0)$  and  $S(3)$  lines also visible in Figure 6 suggests a temperature as high as  $\sim 5000$  K. This is comparable to, but somewhat higher than,  $\text{H}_2$  temperatures seen in other star formation PDRs (Allers et al. 2005) or low-mass  $\text{H}_2$  jets (Caratti o Garatti et al. 2006), approaching the typical  $T_e \sim 8000$  K for Galactic HII regions (Shaver et al. 1983), and is perhaps indicative of the relative youth of the compact HII region in BY72, and/or the hardness of the UV radiation field from the young stars in the HII region.

Another remarkable feature of the IR imaging is the apparent deficit in line emission from the exact peak of the mm-molecular emission (within the pointing uncertainty). Unfortunately a spectrum for this position is not available, since it coincides with emission in the reference beam (the horizontal black line in Fig. 6 at pixel coordinate 420). Thus while we cannot obtain any IR line ratios here with the current data, it appears as if the  $\text{H}_2$   $v=2\rightarrow 1$  and Br- $\gamma$  are both seen in absorption at this peak, creating an apparent “absorption nebula”. This nebula can be seen in Figure 5a as a green patch to the left (Galactic east) of the HII region, since there the blue ( $\text{H}_2$   $v=2\rightarrow 1$ ) and red (Br- $\gamma$ ) appear more strongly “absorbed”, while the green ( $\text{H}_2$   $v=1\rightarrow 0$ ) is only weakly “absorbed”. While much of this appearance may be due to the construction of the RGB image, at the very least it is likely that there is either unusual, highly localised IR emission/absorption at the molecular peak, or that the deeply embedded stars at that position have very unusual IR colours. Moreover, this positional coincidence is highly suggestive. Further east of the peak of the absorption nebula, there seems to be a weaker, comma-shaped extension, and this shape is also seen in some of the  $\text{HCO}^+$  channel maps.

If this “absorption” were real and not an imaging artefact, then it would imply very large columns of gas,  $\sim 10^{24}$   $\text{cm}^{-2}$ . The  $\text{HCO}^+$  self-absorption and spatial distribution require the same condition, and so the implication of very high column density at the molecular peak would seem to be strong. This is also supported when we note that the continuum emission

of the three stars closest to the “absorption nebula” position in Figure 6 (i.e., the bright horizontal lines at pixels 400, 435, and 460) show a very strong attenuation at the shorter  $K$ -band wavelengths, presumably due to severe reddening in the molecular core. Such reddening is not apparently affecting the stars in the HII region (e.g., those labelled A, B, & C in Fig. 6).

The  $K$ -continuum image reveals details of clustering in BY72. Compared to the surrounding sky away from any  $\text{HCO}^+$  emission, within the HII region there is clearly an overabundance of stars. In addition, the bright  $\text{H}_2$  nebulosity immediately to the east of the HII region contains an even more compact clustering of brighter stars, and there is another tight grouping around the molecular peak. To the north and south of the molecular peak, the star density is actually lower than the surroundings, suggesting that here the dust column density is still so high that background stars are being extinguished at  $2\mu\text{m}$ . It is clear that many young stars, some massive enough to form an HII region, have already formed in BY72, and that further star formation appears to be proceeding vigorously to the east of this HII region.

### 3.4. Theoretical Considerations

We note that the typical projected separation of the stars in the central IR groups,  $\sim 2''$  or 4400 AU, is somewhat less than the Jeans length

$$\begin{aligned}
 R_{\text{Jeans}} &\sim \left( \frac{kT_{\text{ex}}}{G(\mu m_{\text{H}})^2 n_{\text{H}_2}} \right)^{0.5} \\
 &\sim 9100 \text{ AU} \left( \frac{T}{30 \text{ K}} \right)^{0.5} \left( \frac{n_{\text{H}_2}}{3 \times 10^5 \text{ cm}^{-3}} \right)^{-0.5}
 \end{aligned} \tag{7}$$

in the dense core, although more extreme local conditions, especially near the centre, may make these scales more commensurate. This disparity is typical of massive clusters (e.g. Churchwell 2002) and is a well-known feature of such regions that models must reproduce. Currently, theories attempt to model this structure using either competitive processes (such as coalescence, e.g. Bonnell et al. 2003) or a scaled up accretion disk/turbulent core scenario (e.g., McKee & Tan 2003). BY72 promises to be a useful test case in this debate, but as indicated by the small value for the dense gas filling factor from §3.2, will require mm-interferometric imagery that approaches the IR resolution. At this level ( $\sim 1''$  or better) we begin to match (at the distance of BY72) the spatial resolution ( $\sim 0.01 \text{ pc}$ ) in the simulations of (e.g.) Banerjee & Pudritz (2007). High-resolution maps of the gas velocity field and linewidth will then help to discriminate between the competing theories.

From the current mm and FIR data we can say that the line emission pattern, derived velocity field, and mass infall rate in BY72 are consistent with the detailed MHD simulations of Banerjee & Pudritz (2007) and radiative transfer treatment of Zhou et al. (1993) for protostars, as well as with the treatment of McKee & Tan (2003). However in this case (a) there are multiple protostellar objects within the collapse zone, rather than a single, more massive one, and (b) the canonical spectral energy distribution of low-mass Class 0 protostars (André et al. 2000) has the flux dropping to undetectable levels at wavelengths shortward of  $10\mu\text{m}$ , although this is under the assumption of spherical symmetry. In BY72 there are a number of near-IR sources visible at the centre of the infalling core, so it is likely that orientation effects play a role in the emergent SED for massive protostars, and/or that the SED evolution is different in the massive protostar case. Again, higher-resolution mm- and FIR-continuum images of the cluster sources will help delineate SED evolution in these massive protostars.

Furthermore, this ongoing star formation is happening within a large-scale infall region ( $\sim 1\text{pc}$ ), and to our knowledge this is the first time that such a coincidence of phenomena has been seen. With so much gas still infalling, it is possible that BY72 could form many more stars before the supply of material is consumed. Dividing the core’s mass by the infall rate gives a maximum lifetime  $t \sim 2 \times 10^5\text{yr}$  for the supply of raw material for new stars, although if a protostar massive enough to develop its own HII region ionises the gas and arrests the infall, the cluster’s formation may be complete in much less time. This timescale is also consistent with the models of (e.g.) McKee & Tan (2003).

Given all the above, we claim that the molecular and IR observations of BY72 indicate the existence of a dense core undergoing global gravitational infall, similar to the case for NGC 2264C (Peretto et al. 2006). We further suggest that, on the basis of the size, mass, luminosity, rate of infall, and near-IR appearance, BY72 is in the process of forming a massive protocluster. The global mass infall rate as determined from the Mopra mm observations is very high even for a massive protostar,  $(2.4 \pm 0.7) \times 10^{-2} M_{\odot} \text{yr}^{-1}$ . To our knowledge, the upper end of this range would be unprecedented, if confirmed.

#### 4. Conclusions

From Mopra and ASTE  $\text{HCO}^+$  observations, the Galactic source G286.21+0.17 (which we also call BY72 from the CHaMP survey master list) has been found to be a massive dense molecular core exhibiting clear signs of gravitational infall. The size and scale of this infall,  $dM/dt \sim 2.4 \times 10^{-2} M_{\odot} \text{yr}^{-1}$  over  $\sim 1\text{pc}$ , is either a record or close to it, and may indicate the global formation of a massive protocluster. AAT near-IR imaging confirms the existence

of unusual spectral signatures and a deeply embedded cluster of stars in the infall zone, as well as an adjacent compact HII region and young star cluster. With an implied beam-filling factor  $\sim 0.1$  in the molecular maps, higher-resolution mm-wave and FIR/MIR observations of this source are encouraged, since it appears to be an exemplary test case for confronting competing theories of massive star formation.

Users of the Mopra telescope have benefited immensely from the efforts of a great many people over the last several years, including the talented and dedicated engineers and scientists at the ATNF, and the staff and students of the Star Formers group within the School of Physics at the University of New South Wales. Because of these efforts, use of this facility has changed over this period from being a difficult exercise to a real pleasure. We would also like to acknowledge the members of the ASTE team for the operation and ceaseless efforts to improve ASTE. This work was financially supported in part by Grant-in-Aid for Scientific Research (KAKENHI) on Priority Areas from the Ministry of Education, Culture, Sports, Science, and Technology of Japan (MEXT), No. 15071205.

PJB gratefully acknowledges support from the School of Physics at the University of Sydney and through NSF grant AST-0645412 at the University of Florida. AMH acknowledges support provided by the Australian Research Council (ARC) in the form of a QEII Fellowship (DP0557850). YM acknowledges financial supports by the research promotion scholarship from Nagoya University and research assistantships from the 21st Century COE Program “ORIUM” (The Origin of the Universe and Matter: Physical Elucidation of the Cosmic History) and the Global COE program “Quest for Fundamental Principles in the Universe: from Particles to the Solar System and the Cosmos”, MEXT, Japan.

*Facilities:* Mopra (MOPS), AAT (IRIS2), ASTE

## REFERENCES

- Allers K N, Jaffe D T, Lacy J H, Draine B T, & Richter M J 2005, ApJ, 630, 368
- André, P., Ward-Thompson, D., & Barsony, M. 2000, in Protostars and Planets IV, eds. Mannings, V., Boss, A. P., Russell, S. S. (Tucson: U. of Arizona Press), p59
- Banerjee R & Pudritz R E 2007, ApJ, 660, 479
- Barnes, D.G. and 38 co-authors 2001, MNRAS, 322, 486
- Barnes, P.J., Crutcher, R., Bieging, J., Willner, S.P., & Storey, J.W.V. 1989, ApJ, 342, 883

- Barnes, P.J., & Crutcher, R. 1990, *ApJ*, 351, 176
- Barnes P.J., Yonekura Y, Miller A, Mhlegger M, Agars L, Wong T, Ladd E F, Mizuno N, & Fukui Y 2006, in *IAU Symposium 231: Astrochemistry Throughout the Universe*, D. Lis, G.A. Blake, E. Herbst (eds.) (Cambridge UP: Cambridge)
- Barnes P J, Yonekura Y, & Fukui Y 2008, *The Galactic Census of High- and Medium-mass Protostars II. Mopra HCO+ and H13CO+ Maps and Analysis*, in prep.
- Beltrán M T, Cesaroni R, Codella C, Testi L, Furuya R S, & Olmi L 2006, *Nature*, 443, 427
- Bonnell I A, Bate M R, & Vine S G 2003, *MNRAS*, 343, 413
- Bronfman L, Nyman L-, & May J 1996, *A&AS*, 115, 81
- Burton, M G 1987, PhD Thesis, University of Edinburgh, unpublished
- Caratti o Garatti A., Giannini T., Nisini B., & Lorenzetti D. 2006, *A&A*, 449, 10771088
- Caselli P, Walmsley C M, Zucconi A, Tafalla M, Dore L, & Myers P C 2002, *ApJ*, 565, 344
- Cavanagh, B., Hirst, P., Jenness, T., Economou, F., Currie, M. J., Todd, S., & Ryder, S. D. 2003, in *ASP Conf. Ser.*, 295, *Astronomical Data Analysis Software and Systems XII*, eds. H. E. Payne, R. I. Jedrzejewski, & R. N. Hook (San Francisco: ASP), 237
- Churchwell, E. 2002, *ARAA*, 40, 27
- Clemens, D.P. 1985, *ApJ*, 295, 422
- Crutcher, R. M. 1999, *ApJ*, 520, 706
- Dutra C M, Bica E, Soares J, & Barbuy B 2003, *A&A*, 400, 533
- Ezawa, H., Kawabe, R., Kohno, K., & Yamamoto, S. 2004, *Proc. SPIE*, 5489, 763
- Faundez S, Bronfman L, Garay G, Chini R, Nyman L-, & May J 2004, *A&A*, 426, 97
- Fuller G A, Williams S J, & Sridharan T K 2005, *A&A*, 442, 949
- Garrod R T, Widicus-Weaver S L, & Herbst E 2008, *ApJ*, 682, 283
- Haese N N & Woods R C 1979, *Chem. Phys. Letters*, 61, 396
- Kamazaki, T., Ezawa, H., Tatematsu, K., Yamaguchi, N., Kuno, N., Morita, K., Yanagisawa, K., Horigome, O., & Maekawa, J. 2005, *ASP Conf. Ser.*, 347, 533



- Kohno, K., and 41 co-authors 2004, in *The Dense Interstellar Medium in Galaxies*, ed. S. Pfalzner et al. (Berlin: Springer), 349
- Kohno, K. 2005, *ASP Conf. Ser.*, 344, 242
- Lada, C. J. 1999, in *The Origin of Stars and Planetary Systems*, ed. C. J. Lada & N. D. Kylafis (Dordrecht: Kluwer), 143
- Ladd E. F., Purcell C. R., Wong T., & Robertson S., 2005, *PASA*, 22, 62
- Lee J-E, Evans N J, Shirley Y L, & Tatematsu K 2003, *ApJ*, 583, 789
- Longmore S N, Burton M G, Barnes P J, Wong T, Purcell C R, & Ott J 2007, *MNRAS*, 535, 572
- Loren R B, Wootten A, Wilking B A 1990, *ApJ*, 365, 269
- Mac Low, M.-M., & Klessen, R. S. 2004, *Rev. Mod. Phys.*, 76, 125
- McKee C F & Tan J C 2003 *ApJ*, 585, 850
- Merrifield, M. 1992, *AJ*, 103, 1552
- Murphy T, Mauch T, Green A, Hunstead RW, Piestrzynska B, Kels AP, & Sztajer P 2007, *MNRAS*, 382, 382
- Myers P C, Mardones D, Tafalla M, Williams J P, Wilner D J 1996, *ApJLett*, 465, L133
- Nakamura F & Li Z-Y 2005 *ApJ*, 631, 411
- Peretto N, Andr P, & Belloche A 2006, *A&A*, 445, 979
- Ryder, S. D., Sun, Y.-S., Ashley, M. C. B., Burton, M. G., Allen, L. E., & Storey, J. W. V. 1998, *PASA*, 15, 228
- Shaver, P. A., McGee, R. X., Newton, L. M., Danks, A. C., & Pottasch, S. R. 1983, *MNRAS*, 204, 53
- Schilke, P., Groesbeck, T. D., Blake, G. A., & Phillips, T. G. 1997, *ApJS*, 108, 301337
- Shu F 1977 *ApJ*, 214, 488
- Sorai, K., Sunada, K., Okumura, S.K., Iwasa, T., Tanaka, A., Natori, N., & Onuki, H. 2000, *Proc. SPIE*, 4015, 86

- Spitzer, L. 1978, *Physical Processes in the Interstellar Medium* (Wiley: New York)
- Sridharan T K, Beuther H, Schilke P, Menten K M, & Wyrowski F 2002, *ApJ*, 566, 931
- Tej A., Ojha D. K., Ghosh S. K., Kulkarni V. K., Verma R. P., Vig S., & Prabhu T. P. 2006, *A&A*, 452, 203215
- Tinney, C. G., Ryder, S. D., Ellis, S. C., Churilov, V., Dawson, J., Smith, G., Waller, L., Whittard, J., Haynes, R., Lankshear, A., Barton, J. R., Evans, C. J., Shortridge, K., Farrell, T., & Bailey, J. 2004, in *Proc. SPIE*, 5492, 998
- Townes C.H. & Schawlow A.L. 1975, *Microwave Spectroscopy* (Dover: New York)
- Wilson W, Müller E, & Ferris D 2006, *ATNF Newsletter*, no. 59, [www.atnf.csiro.au/news/news-letter/jun06/](http://www.atnf.csiro.au/news/news-letter/jun06/)
- Yonekura Y, Asayama S, Kimura K, Ogawa H, Kanai Y, Yamaguchi N, Barnes P J, & Fukui Y 2005, *ApJ*, 634, 476
- Yonekura Y, Barnes P J, & Fukui Y 2008, *The Galactic Census of High- and Medium-mass Protostars I. Master Source List and Nanten C18O and HCO+ Maps*, in prep.
- Zhou S., Evans N.J.II, Kmpe C., & Walmsley C.M. 1993, *ApJ*, 404, 232

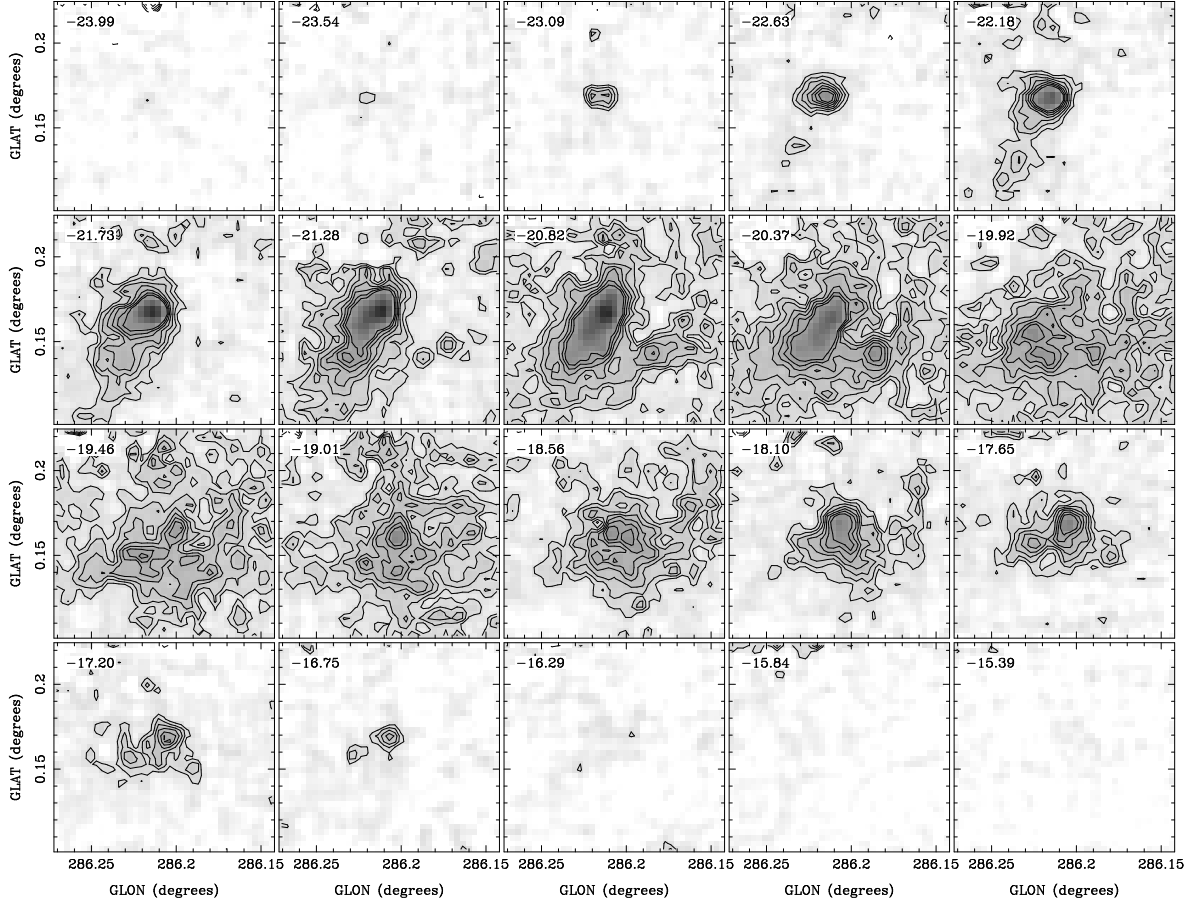


Fig. 1.— Mopra channel maps of  $\text{HCO}^+ J=1 \rightarrow 0$  emission from an inner  $7'$ -field of  $\text{BY72} = \text{G286.21} + 0.17$ , shown on the  $T_A^*$  scale;  $T_R^* = T_A^*/0.7$ . Each panel is actually the mean of four  $0.11 \text{ km s}^{-1}$  wide channels, hence the panel spacing of  $0.45 \text{ km s}^{-1}$ . The grey scale is linear from  $0 \text{ K}$  to the peak at  $2.19 \text{ K}$ , while the contour levels are from 3 to 9 times the rms noise level for each panel, which is  $0.092 \text{ K}$ . At a distance of  $2.2 \text{ kpc}$ , the scale is  $10'' = 0.107 \text{ pc}$  or  $0.5 \text{ pc} = 47''$ .

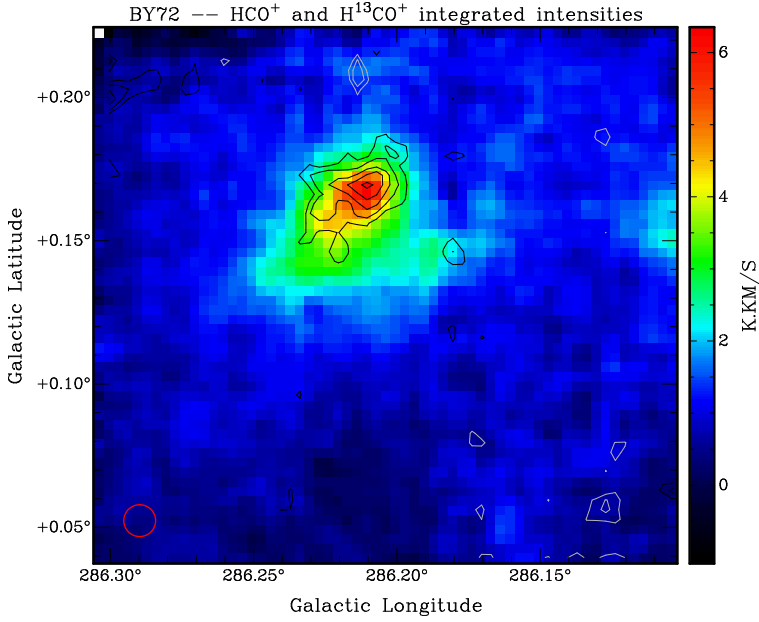


Fig. 2.— (*Image*) Wider 11'-field of Mopra  $\text{HCO}^+$   $J=1\rightarrow 0$  integrated intensity from BY72, on the  $T_A^*$  scale as given by the colourbar. (This figure is in colour in the online version of the *Journal*.) The integration is over the range  $-23.20$  to  $-16.63$   $\text{km s}^{-1}$  or 58 channels, yielding an rms noise level  $0.16$   $\text{K km s}^{-1}$ : hence the widespread low-level emission above  $\sim 0.5$   $\text{K km s}^{-1}$  is real. (*Contours*) Mopra  $\text{H}^{13}\text{CO}^+$   $J=1\rightarrow 0$  integrated intensity in  $T_A^*$ , levels are (*grey*)  $-0.5$ ,  $-0.35$ , (*black*)  $0.35$ ,  $0.5$ ,  $0.7$ ,  $0.9$ , and  $1.1$   $\text{K km s}^{-1}$ . The integration is from  $-21.94$  to  $-17.86$   $\text{km s}^{-1}$ , giving an rms noise level  $0.12$   $\text{K km s}^{-1}$ . The smoothed Mopra HPBW for both datasets is shown for reference in the lower-left corner.

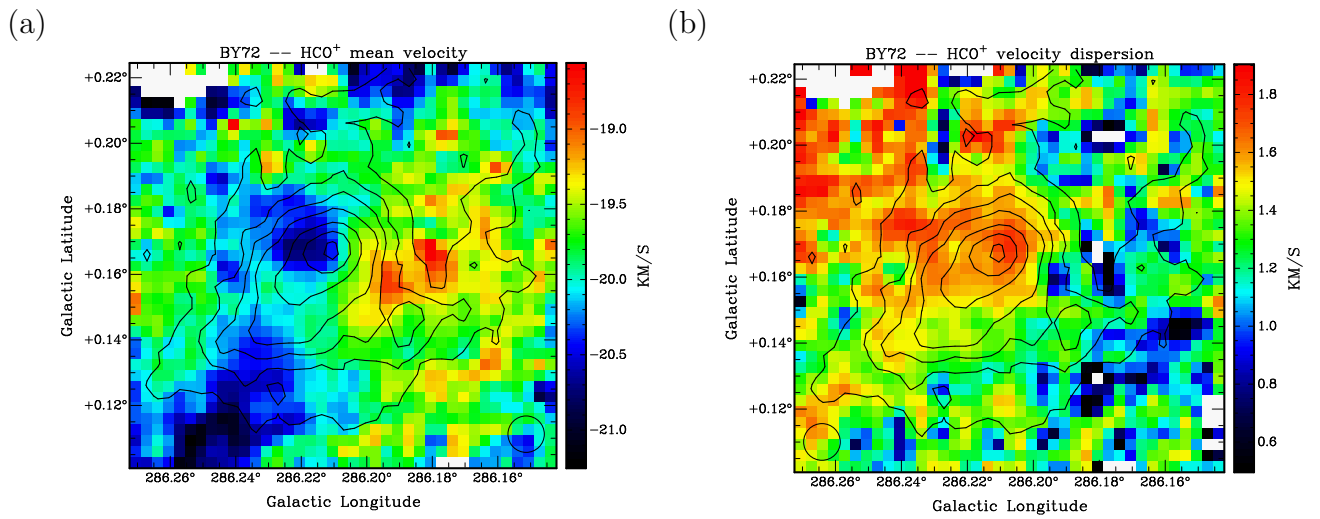


Fig. 3.— Moment images of BY72 from the Mopra HCO<sup>+</sup> data with telescope beam as shown in the corners, and overlaid with HCO<sup>+</sup> integrated intensity contours at 1.35, 1.9, 2.4, 3.0, 4.0, 5.0, and 6.0 K km s<sup>-1</sup> ( $\sigma = 0.16$  K km s<sup>-1</sup>). (This figure is in colour in the online version of the *Journal*.) All moments for HCO<sup>+</sup> were calculated over the same velocity range as in Fig. 2(*image*). (a) First moment (intensity-weighted mean velocity field). (b) Second moment (velocity dispersion).

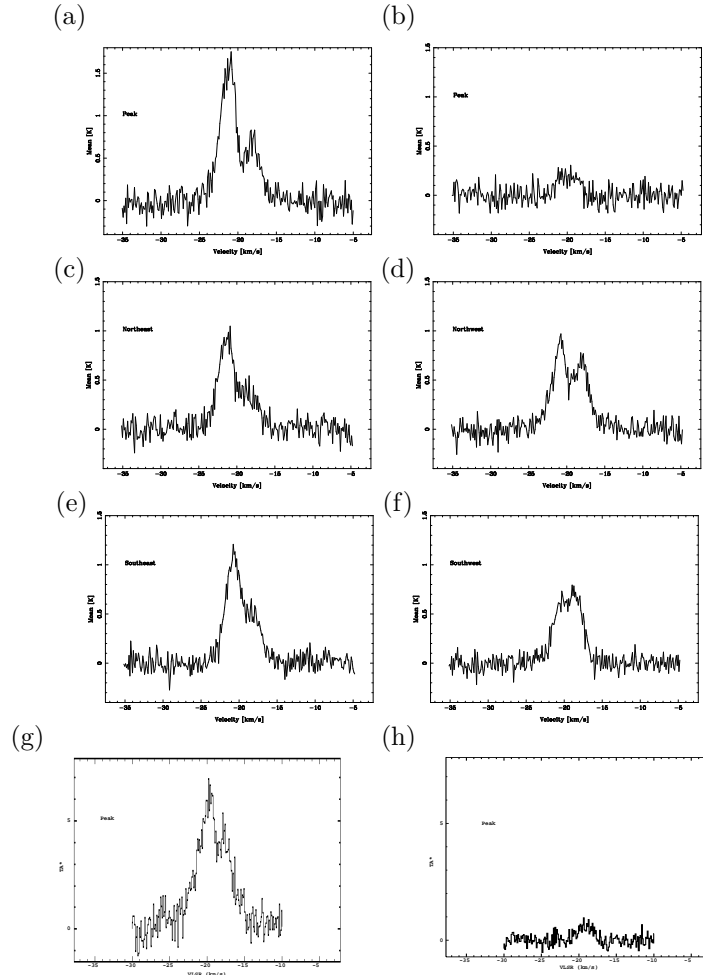


Fig. 4.— Sample Mopra and ASTE spectra of BY72. Panels *a* and *b* are Mopra  $J=1\rightarrow 0$  mean spectra from a beam-sized area around the peak position of BY72 in  $\text{HCO}^+$  and  $\text{H}^{13}\text{CO}^+$ , respectively. Panels *c*–*f* are Mopra  $\text{HCO}^+$   $J=1\rightarrow 0$  mean spectra from similar areas in the indicated quadrants around the peak position. Panels *g* and *h* are ASTE  $J=4\rightarrow 3$  spectra from the BY72 peak position in  $\text{HCO}^+$  and  $\text{H}^{13}\text{CO}^+$ , respectively.

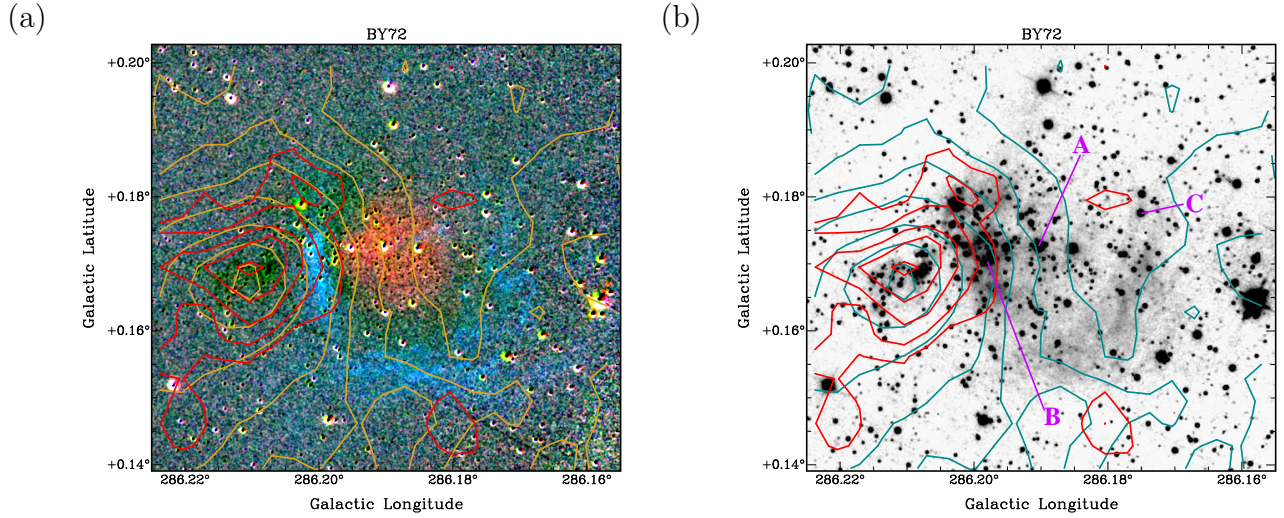


Fig. 5.— (a) RGB-pseudocolour image of BY72 in  $K$ -band spectral lines. Here Br- $\gamma$  is shown as red, and  $H_2 S(1)$  is shown as green ( $v=1 \rightarrow 0$ ) & blue ( $v=2 \rightarrow 1$ ). Contours are overlaid from Mopra  $HCO^+$  (*gold*) and  $H^{13}CO^+$  (*red*) integrated intensities (levels as in Figs. 3 & 2, resp.). (b) Same contours levels as *a*, but now coloured *blue* and *red*, and overlaid on the  $K$ -continuum image. The stars from Fig. 6 are labelled in magenta.

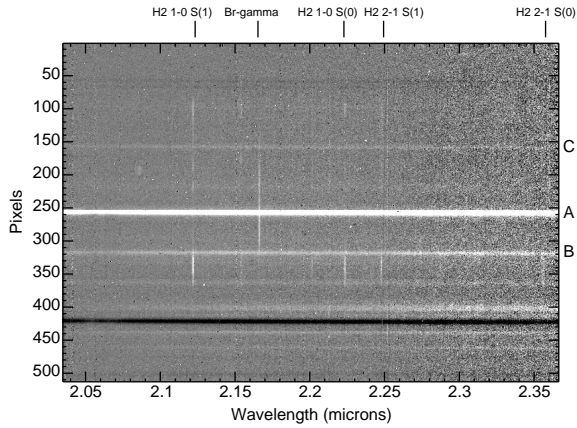


Fig. 6.— Near-IR long-slit spectrum across BY72, where the slit was oriented along a line joining the peak of the HII/Br- $\gamma$  emission (to the NW of Fig. 5 at the top of this figure) and the peak of the  $HCO^+$  emission (to the SE of Fig. 5 at the bottom of this figure). The spectral lines are as indicated, and the labels A, B, and C refer to stars similarly labelled in Fig. 5.